

Fully Band Resolved Scattering Rate in MgB₂ Revealed by Nonlinear Hall Effect and Magnetoresistance Measurements

Huan Yang¹, Yi Liu¹, Chenggang Zhuang^{2,3,4}, Junren Shi^{1,*}, Yugui Yao¹, Sandro Massidda⁵, Marco Monni⁵, Ying Jia¹, Xiaoxing Xi^{3,4}, Qi Li³, Zi-Kui Liu⁴, Qingrong Feng², and Hai-Hu Wen^{1,*}

¹*Institute of Physics and Beijing National Laboratory for Condensed Matter Physics, Chinese Academy of Sciences, P. O. Box 603, Beijing 100080, P. R. China*

²*Department of Physics, Peking University, Beijing 100871, P. R. China*

³*Department of Physics, The Pennsylvania State University, University Park, Pennsylvania 16802, USA*

⁴*Department of Materials Science and Engineering,*

The Pennsylvania State University, University Park, Pennsylvania 16802, USA and

⁵*SLACS-INFN and Dipartimento di Fisica, Università di Cagliari, I-09042 Monserrato (Ca), Italy*

(Dated: October 28, 2018)

We have measured the normal state temperature dependence of the Hall effect and magnetoresistance in epitaxial MgB₂ thin films with variable disorders characterized by the residual resistance ratio RRR ranging from 4.0 to 33.3. A strong nonlinearity of the Hall effect and magnetoresistance have been found in clean samples, and they decrease gradually with the increase of disorders or temperature. By fitting the data to the theoretical model based on the Boltzmann equation and *ab initio* calculations for a four-band system, for the first time, we derived the scattering rates of these four bands at different temperatures and magnitude of disorders. Our method provides a unique way to derive these important parameters in multiband systems.

PACS numbers: 74.70.Ad, 71.15.Dx, 72.10.Di, 74.25.Fy

The multiband character of MgB₂ [1] dominates its properties in both superconducting [2, 3, 4, 5, 6] and normal state [7, 8, 9, 10]. In MgB₂, there are two holelike quasi-two-dimensional σ bands (bonding σ_1 and antibonding σ_2), an “electronlike” antibonding (π_1) and a “holelike” bonding (π_2) three-dimensional π band [11, 12]. The electron scattering rates in each band and between different bands are the most critical parameters dictating all aspects of the properties of MgB₂ [8, 9, 10, 13]. The temperature dependence of the electron scattering rates arises from electron-phonon (e -ph) coupling, and the strong e -ph coupling between the E_{2g} phonon mode and the σ bands are responsible for the high T_c in MgB₂ [14]. Consequently, measuring the intraband and interband scattering rates in MgB₂, with a goal to further manipulate them in order to reveal new physics and achieve desirable properties, has been central to many research studies. The properties used to extract the band-resolved scattering rates include electrical resistivity [10], magnetoresistance (MR) [8, 9, 15, 16], far-infrared spectroscopy [17], and upper critical field H_{c2} [13]. For example, Monni *et al.* was able to derive the temperature-dependent relaxation times, τ_σ and τ_π for the generalized σ and π bands, respectively, from the MR measurement and *ab initio* calculations [15]. However, although the two σ bands (or the two π bands) have similar properties, they are distinct from each other. For example, the two π bands have different types of carriers. Without the knowledge of scattering rates in all the *four* different bands, the understanding of the multiband nature of MgB₂ is incomplete. To our best knowledge, information from MR alone is not sufficient to derive the scattering rates in four different bands. In this Letter,

we report results of strong nonlinear Hall effect (NLHE) and large MR in pure epitaxial MgB₂ films. This made it possible to derive the scattering rates and their dependencies on temperature and disorder in each of the four bands, a significant advancement of the knowledge concerning the multiband character of MgB₂.

The MgB₂ films used in this work were grown by the hybrid physical-chemical vapor deposition (HPCVD) technique [18] on (0001) 6H-SiC substrates. They were epitaxial with a c -axis orientation and the thickness was between 100 and 200 nm. Films with different magnitudes of disorder, thus different residual resistivity, were grown at slightly different temperatures, pressures, and growth rates. Nevertheless, all the films had similar T_c around 40 K and narrow x-ray diffraction rocking curves. The longitudinal and the transverse resistivity were measured with sweeping magnetic field at a fixed temperature or sweeping temperature at a fixed field. All the measurements were performed with magnetic field applied perpendicular to the ab plane of the film. For the seven films investigated here, the residual resistance ratios $RRR \equiv \rho(300 \text{ K})/\rho(41 \text{ K})$ are 33.3, 24.5, 20.9, 14.4, 6.88, 6.4 and 4.0, and we mark them as RRR33.3, RRR24.5, RRR20.9, RRR14.4, RRR9.9, RRR6.4, and RRR4.0, respectively. Their corresponding residual resistivities ρ_n are 0.293, 0.347, 0.411, 0.740, 1.32, 2.55, and 4.66 $\mu\Omega \text{ cm}$, respectively.

In Fig. 1, we show the field dependence of $\Delta\rho_{xx}(B)/\rho_{xx}(0)$ and $R_H(B)/R_H(0)$ for all the seven samples at $T = 41 \text{ K}$. Here $R_H(B) = \rho_{xy}/B$ is the Hall coefficient at the magnetic field B ; ρ_{xx} and ρ_{xy} are the longitudinal and transverse resistivity, and $\Delta\rho_{xx}(B) = \rho_{xx}(B) - \rho_{xx}(0)$. The dashed lines show the cases for

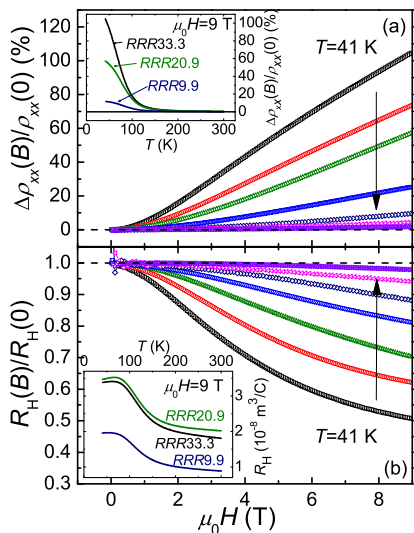


FIG. 1: (Color online) Field dependence of $\Delta\rho_{xx}(B)/\rho_{xx}(0)$ (a), and $R_H(B)/R_H(0)$ (b) at $T = 41$ K for seven samples with RRR values from 33.3 to 4.0 (direction of the arrows). Insets in (a) and (b) shows the temperature dependence of the normalized MR and R_H at 9 T for sample RRR33.3, RRR20.9, and RRR9.9. One can see that the MR and R_H decrease rapidly when the temperature is increased.

zero MR and linear Hall effect, as one can expect in single band metals with the spherical or the columned Fermi surface. MR and NLHE are observed in all the samples, but the MR is larger and the NLHE is stronger in cleaner samples. In sample RRR33.3 at 9 T and 41 K, a large MR of more than 100% is observed, and the Hall coefficient decreases to about half of the zero-field value. The magnitude of MR is similar to an earlier report in a clean MgB_2 film due to the multiband effect.[9] For the dirty samples with low RRR , because the interband scattering is very strong, the multiband natures, such as the MR and the NLHE are weakened, and the Kohler's rule is satisfied [19], which is not the case in clean MgB_2 films.[9] The insets in Fig. 1 (a) and Fig. 1 (b) present the temperature dependence of the normalized MR and NLHE at 9 T of the films RRR33.3, RRR20.9, and RRR9.9. Both MR and the NLHE decrease rapidly with increasing T . In a single band metal with anisotropic Fermi surface, R_H should be very weakly T dependent. However, as shown in the inset of Fig. 1 (b), the Hall coefficient has a strong T dependence, especially for the clean samples. It should be noted that the value of R_H is about an order of magnitude larger than those reported by Eltsev *et al.* in single crystals [20], which is not necessarily an indication of a smaller density of charge carriers in this clean film. As discussed below, due to the existence of multiple bands, the Hall coefficient can no longer be written simply as $1/ne$ as in single band materials.

The large MR and NLHE originate directly from the

multiband character of MgB_2 , from which we can extract information on the electron scattering rates in the different bands. To do this, we first need to determine the contribution of each band to the (Hall) conductivity at the given electron scattering rate. The complex band structure of MgB_2 renders the simple formulae presented in textbooks invalid. We thus employ the semiclassical Boltzmann theory with the relaxation time approximation [21]. In this approximation, the electron state is assumed to have a finite lifetime, which is induced by all possible electron scattering processes, including the intraband and inter-band scatterings. The conductivity tensor σ for the n^{th} band reads:

$$\sigma^{(n)} = e^2 \int \frac{d\mathbf{k}}{4\pi^3} \tau_n \mathbf{v}_n(\mathbf{k}) \bar{\mathbf{v}}_n(\mathbf{k}) \left(-\frac{\partial f}{\partial \varepsilon} \right)_{\varepsilon=\varepsilon_n(\mathbf{k})}, \quad (1)$$

where $\mathbf{v}_n(\mathbf{k}) = \partial \varepsilon_n / \partial \hbar \mathbf{k}$ is the group velocity at the wave vector \mathbf{k} . Under a magnetic field, the wave vector of electron evolves by $\hbar \dot{\mathbf{k}}_n = -(e/c) \mathbf{v}_n(\mathbf{k}) \times \mathbf{B}$; and $\bar{\mathbf{v}}_n(\mathbf{k}) = \int_{-\infty}^0 dt e^{t/\tau_n} \mathbf{v}_n(\mathbf{k}) / \tau_n$, is a weighted average of the velocity over the past history of the electron orbit passing through \mathbf{k} ; f is the Fermi distribution function. Here, we have assumed that τ_n is independent on the wave vector \mathbf{k} . The band structure necessary for the evaluation is determined from the *ab initio* electronic structure calculations. Here we employed the ultrasoft pseudopotential plane-wave method [22] with generalized-gradient approximation [23] for the exchange and correlation potential. For the case of $B = 0$, we obtain the electronic density of state at the Fermi level and plasma frequency ω_{xx} and ω_{zz} for each band in very good agreement with those given by Liu *et al.* [10]. For $B \neq 0$, $\bar{\mathbf{v}}_n$ is obtained by self-adaptive Runge-Kutta integration. The calculated Hall conductivity $\sigma_{xy}^{(n)}/\tau_n$, as a function of $B\tau_n$, is shown in Fig. 2. The calculation results for both σ_{xx} and σ_{xy} can be well interpolated by the Padé series:

$$\begin{aligned} \sigma_{xx}^{(n)}/\tau_n &= \frac{a_1^{(n)} + a_2^{(n)} \cdot (B\tau_n)^2}{1 + b_1^{(n)} \cdot (B\tau_n)^2 + b_2^{(n)} \cdot (B\tau_n)^4}, \\ \sigma_{xy}^{(n)}/\tau_n &= \frac{c_1^{(n)} \cdot (B\tau_n) + c_2^{(n)} \cdot (B\tau_n)^3}{1 + d_1^{(n)} \cdot (B\tau_n)^2 + d_2^{(n)} \cdot (B\tau_n)^4}, \end{aligned} \quad (2)$$

with the coefficients shown in Table I. The total conductivity is the summation of the four bands. The *ab initio* calculation reveals some unexpected behaviors: (i) The “electronlike” π_1 band behaves as a hole band when the magnetic field is normal to the *ab* plane; (ii) The “holelike” band π_2 has a sign change from positive to negative with increasing $B\tau$. The latter can be understood as a result of the complex structure of the π_2 Fermi surface, which is composed of electron-like belly and hole-like hills, as shown in the left inset of Fig. 2. At small $B\tau$, the conduction is dominated by the small orbits around the hills, showing the hole-like behavior. The opposite happens when $B\tau$ is large. These unusual behaviors clearly

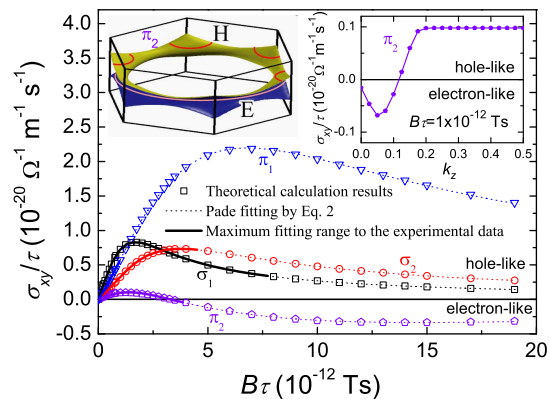


FIG. 2: (Color online) $B\tau$ dependence of σ_{xy}/τ for the four bands. The left inset shows the Fermi surface of π_2 band, the electron-like orbit ('E') around the belly and the hole-like orbit ('H') around the hills are indicated as the arc lines. The right inset shows the partial Hall conductivity $\sigma_{xy}^{(n)}(k_z)/\tau = \frac{e^2}{4\pi^3} \int dk_x dk_y \int_{-k_z}^{k_z} dk'_z v_x^{(n)}(\mathbf{k}) v_y^{(n)}(\mathbf{k}) \left(-\frac{\partial f}{\partial \epsilon}\right)_{\epsilon=\epsilon_n(\mathbf{k})}$ contributed by orbits between $-k_z$ to k_z of π_2 band as a function of k_z . It demonstrates that the contribution from the belly region is negative while the hill region is positive.

TABLE I: Fitting parameters of Fig. 2 using Eq. 2 (All parameters are in SI unit).

σ_{xx}	a_1 (10^{-20})	a_2 (10^4)	b_1 (10^{24})	b_2 (10^{48})
σ_1	1.66990	10.94632	6.76549	2.29927
σ_2	1.69337	0.29735	0.27378	0.01295
π_1	4.95528	2.20045	0.51383	0.00998
π_2	1.88788	0.32211	0.26752	0.00269
σ_{xy}	c_1 (10^{-8})	c_2 (10^{16})	d_1 (10^{24})	d_2 (10^{48})
σ_1	0.92146	2.59031	2.90378	0.93769
σ_2	0.28948	0.41532	1.08441	0.07650
π_1	0.45035	1.46465	2.26895	0.04918
π_2	0.12735	-0.01163	0.20542	0.00127

indicate the inapplicability of the simple formula in describing the magnetoresistance of MgB_2 system [8].

By using the least-square fit to multi-functions [24], we then fit the experimental data $\sigma_{xx}(B)$ and $\sigma_{xy}(B)$ (derived from the resistivity by $\sigma_{xx} \equiv \rho_{xx}/(\rho_{xx}^2 + \rho_{xy}^2)$ and $\sigma_{xy} \equiv \rho_{xy}/(\rho_{xx}^2 + \rho_{xy}^2)$) at each temperature to Eq. 2 by adjusting the four electron scattering times. The maximum range of $B\tau$ in the fitting are plotted by the thick solid lines as shown in Fig. 2. Figure 3 shows the temperature dependence of four scattering times for samples RRR33.3 and RRR20.9. Note that the fitting becomes less reliable at high temperature ($T > 100\text{K}$), as the non-linearity of the magneto-resistivity becomes weaker.

To extend our fitting to higher temperature, we adopt a global fitting approach: Instead of fitting an indi-

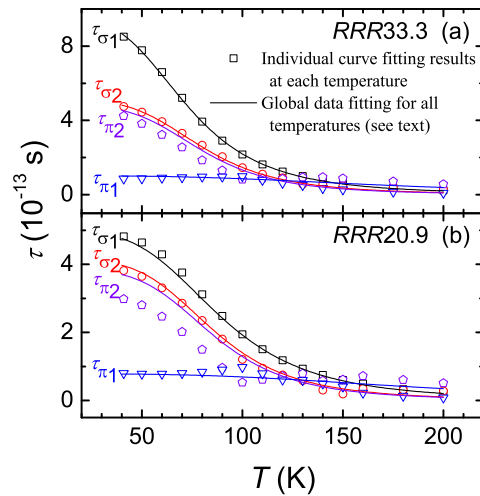


FIG. 3: (Color online) Temperature dependence of calculated transport scattering times of the four bands for MgB_2 films RRR33.3 (a), and RRR20.9 (b).

vidual curve at a time, we simultaneously fit all the curves for all temperatures. To do that, we assume $1/\tau^{(n)} = 1/\tau_{\text{imp}}^{(n)} + 1/\tau_{e\text{-ph}}^{(n)}(T)$, where $\tau_{\text{imp}}^{(n)}$ is the scattering time from impurities and is T -independent, and $\tau_{e\text{-ph}}^{(n)}(T)$ is due to the e -ph coupling, and can be modeled as $1/\tau_{e\text{-ph}}^{(n)}(T) = \alpha_n T^{\beta_n}$. The results are shown by the solid lines in Fig. 3. We find that both approaches coincide well.

We can separate the T -independent impurity contribution with the T -dependent e -ph contribution. In Fig. 4, we plot the temperature dependence of $1/\tau_{e\text{-ph}}$ of three clean samples RRR33.3, RRR24.9, and RRR20.9. The values from all the three samples are close to each other, indicating the e -ph coupling are not strongly affected by the impurities. The exponents β_n for the temperature dependence of $1/\tau_{e\text{-ph}}$ are found to be 3.80 (σ_1), 4.15 (σ_2), 4.22 (π_1), and 3.12 (π_2), respectively. This is in accordance with the expectation of theory [25]. The results clearly show that the σ bands have stronger e -ph coupling than the π_1 band, in agreement with the theoretical calculation [15]. Surprisingly, the e -ph coupling in the π_2 band is also very strong. The difference between the e -ph coupling in the two π bands can be understood by our *ab initio* calculation: in the fitting range shown in Fig. 2, the magneto-transport of π_2 band is dominated by the hills of its Fermi surface, while that of the π_1 band is dominated by the belly (see insets of Fig. 2). Momentum changes to back-scatter an electron in the hills of π_2 band, as well as in the two sigma ones, are much smaller than that in the π_1 band. As a result, phonon is much more effective in scattering electrons in π_2 and two σ bands than in π_1 . The intriguing result cannot be

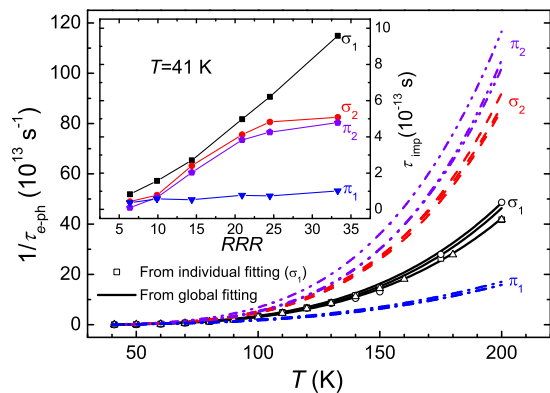


FIG. 4: (Color online) Temperature dependence of $1/\tau_{e-ph}$ of four bands for three different samples RRR33.3, RRR24.5, and RRR20.9. The inset shows the correlation between the scattering time from the impurities and RRR for seven different samples.

revealed without our fully band-resolved method.

The inset to Fig. 4 shows the dependence of the impurity scattering rate on RRR . It shows that disorder affects the impurity scattering much more strongly in the σ bands and π_2 band than in the π_1 band. The calculation results show that for the dirty sample RRR6.4, the scattering times for the four bands are comparable.

In conclusion, we have observed large magnetoresistance and nonlinear Hall effect in clean MgB_2 films, from which we have calculated the scattering times of each one of the four bands, in the aid of theory based on the Boltzmann equation and *ab initio* calculations. Surprisingly, the π_2 band seems to be similar as the two σ bands, i.e., has a large scattering time in pure samples at low temperature, and also has a strong $e-ph$ coupling. And the electron-phonon scattering is much weaker in the π_1 band than other three bands, making the π_1 band the least scattered at high temperatures. This may be caused by the different structure of the Fermi surface of this band. Disorder modifies the multiband electron scattering much in the same way as the phonon, reducing the scattering times of the two σ bands and π_2 band to be comparable to the π_1 band. This detailed knowledge on the band-resolved scattering rates allow to have deeper insight on the properties of MgB_2 than using the two-band approximation.

We thank A. Gurevich, I. I. Mazin, M. Putti, C. Ferdeghini for critical remarks and helpful discussions. This work is supported by the Natural Science Foundation of China, the MOST Project (Nos. 2006CB601000, 2006CB921802, 2006CB921300, 2007CB925000), the Knowledge Innovation Project of Chinese Academy of Sciences (ITSNEM). The work at Penn State is sup-

ported by NSF under Grant Nos. DMR-0306746 (X. X. X.), DMR-0405502 (Q. L.), and DMR-0514592 (Z. K. L. and X. X. X.), and by ONR under Grant No. N00014-00-1-0294 (X. X. X.). Work in Italy is supported by MIUR, PRIN2006021741, and PON-CyberSar (COSMOLAB).

*Corresponding authors: experiment and data analysis: hhwen@aphy.iphy.ac.cn (H. H. Wen); theory: jrshi@aphy.iphy.ac.cn (J. R. Shi).

- [1] P. C. Canfield and G.W. Crabtree, Phys. Today 56, No. 3, 34 (2003).
- [2] A. Rydh *et al.*, Phys. Rev. B **70**, 132503 (2004); A. E. Koshelev and A. A. Golubov, Phys. Rev. Lett. **92**, 107008 (2004); A. A. Golubov and A. E. Koshelev, Phys. Rev. B **68**, 104503 (2003).
- [3] H. J. Choi *et al.*, Nature (London) **418**, 758 (2002).
- [4] H. Yang *et al.*, Phys. Rev. B **76**, 134513 (2007).
- [5] R. S. Gonnelli *et al.*, Phys. Rev. Lett. **89**, 247004 (2002).
- [6] M. R. Eskildsen *et al.*, Phys. Rev. Lett. **89**, 187003 (2002).
- [7] P. de la Mora, M. Castro, and G. Tavizon, J. Phys.: Condens. Matter **17**, 965 (2005).
- [8] I. Pallecchi *et al.*, Phys. Rev. B **72**, 184512 (2005); I. Pallecchi *et al.*, Eur. Phys. J. B **52**, 171 (2006).
- [9] Q. Li *et al.*, Phys. Rev. Lett. **96**, 167003 (2006).
- [10] A. Y. Liu, I. I. Mazin, and J. Kortus, Phys. Rev. Lett. **87**, 087005 (2001); I. I. Mazin *et al.*, *ibid* **89**, 107002 (2002).
- [11] J. Kortus *et al.*, Phys. Rev. Lett. **86**, 4656 (2001).
- [12] E. A. Yelland *et al.*, Phys. Rev. Lett. **88**, 217002 (2002).
- [13] A. Gurevich, Phys. Rev. B **67**, 184515 (2003).
- [14] S. L. Bud'ko *et al.*, Phys. Rev. Lett. **86**, 1877 (2001); D. G. Hinks, H. Claus, and J. D. Jorgensen, Nature (London) **411** 457 (2001).
- [15] M. Monni *et al.*, Europhys. Lett. **81**, 67006 (2008).
- [16] V. Ferrando, *et al.*, J. Appl. Phys. **101**, 043903 (2007).
- [17] M. Ortolani, *et al.*, Phys. Rev. B **71**, 172508 (2005).
- [18] X. H. Zeng *et al.*, Nature Mater. **1**, 35 (2002); C. G. Zhuang *et al.*, J. Appl. Phys. **104**, 013924 (2008).
- [19] S. L. Bud'ko, *et al.*, Phys. Rev. B **63**, 220503(R) (2001).
- [20] Yu. Eltsev *et al.*, Phys. Rev. B **66**, 180504(R) (2002).
- [21] N. W. Ashcroft and N. D. Mermin, *Solid State Physics* (Harcourt: Orlando, 1976).
- [22] Z. Fang and K. Terakura, J. Phys.: Conf. Matt. **14**, 3001(2002).
- [23] J. P. Perdew, K. Burke, and M. Ernzerhof, Phys. Rev. Lett. **77**, 3865(1996).
- [24] P. R. Bevington and D. K. Robinson, *Data Reduction and Error Analysis for the Physical Sciences* (McGraw-Hill Inc., New York, 2003).
- [25] For the simple metals, the low temperature $e-ph$ transport scattering rate follows the so-called "Bloch T^5 law". However, for systems with complex Fermi surfaces or small Fermi pockets, the back-scattering of electron may not require large momentum transfer, and the transport scattering rate will be proportional to T^3 . In general, the exponent should be in the range of 3-5. See Ref. [21].